1521-0103/374/2/252–263$35.00
THE JOURNAL OF PHARMACOLOGY AND EXPERIMENTAL THERAPEUTICS

https://doi.org/10.1124/jpet.120.266122
J Pharmacol Exp Ther 374:252–263, August 2020

MK-8719, a Novel and Selective *O*-GlcNAcase Inhibitor That Reduces the Formation of Pathological Tau and Ameliorates Neurodegeneration in a Mouse Model of Tauopathy[S]

Xiaohai Wang, Wenping Li, Jacob Marcus, Michelle Pearson, Lixin Song, Karen Smith, Giuseppe Terracina, Julie Lee, Kwok-Lam Karen Hong, Sherry X. Lu, Lynn Hyde, Shu-Cheng Chen, David Kinsley, Jerry P. Melchor, Daniel J. Rubins, Xiangjun Meng, Eric Hostetler, Cyrille Sur, Lili Zhang, Joel B. Schachter, J. Fred Hess, Harold G. Selnick, David J. Vocadlo, Ernest J. McEachern, Jason M. Uslaner, Joseph L. Duffy, and Sean M. Smith

MRL, Merck & Co., Inc., Kenilworth, New Jersey (X.W., W.L., J.M., M.P., L.S., K.S., G.T., J.L., K.-L.K.H., S.X.L., L.H., S.-C.C., D.K., J.P.M., D.J.R., X.M., E.H., C.S., L.Z., J.B.S., J.F.H., H.G.S., J.M.U., J.L.D., S.M.S.) and Alectos Therapeutics Inc., Burnaby, British Columbia, Canada (D.J.V., E.J.M.)

Received March 6, 2020; accepted June 1, 2020

ABSTRACT

Deposition of hyperphosphorylated and aggregated tau protein in the central nervous system is characteristic of Alzheimer disease and other tauopathies. Tau is subject to *O*-linked *N*-acetylglucosamine (*O*-GlcNAc) modification, and *O*-GlcNAcylation of tau has been shown to influence tau phosphorylation and aggregation. Inhibition of *O*-GlcNAcase (OGA), the enzyme that removes *O*-GlcNAc moieties, is a novel strategy to attenuate the formation of pathologic tau. Here we described the in vitro and in vivo pharmacological properties of a novel and selective OGA inhibitor, MK-8719. In vitro, this compound is a potent inhibitor of the human OGA enzyme with comparable activity against the corresponding enzymes from mouse, rat, and dog. In vivo, oral administration of MK-8719 elevates brain and peripheral blood mononuclear cell *O*-GlcNAc levels in a dose-dependent manner. In addition, positron emission tomography imaging studies demonstrate robust target engagement of MK-8719 in the brains of rats and rTg4510 mice. In the rTg4510 mouse model of human tauopathy, MK-8719 significantly increases brain *O*-GlcNAc levels and reduces pathologic tau. The reduction in tau pathology in rTg4510 mice is accompanied by attenuation of brain atrophy, including reduction of forebrain volume loss as revealed by volumetric magnetic resonance imaging analysis. These findings suggest that OGA inhibition may reduce tau pathology in tauopathies. However, since hundreds of *O*-GlcNAcylated proteins may be influenced by OGA inhibition, it will be critical to understand the physiologic and toxicological consequences of chronic *O*-GlcNAc elevation in vivo.

SIGNIFICANCE STATEMENT

MK-8719 is a novel, selective, and potent *O*-linked *N*-acetylglucosamine (*O*-GlcNAc)-ase (OGA) inhibitor that inhibits OGA enzyme activity across multiple species with comparable in vitro potency. In vivo, MK-8719 elevates brain *O*-GlcNAc levels, reduces pathological tau, and ameliorates brain atrophy in the rTg4510 mouse model of tauopathy. These findings indicate that OGA inhibition may be a promising therapeutic strategy for the treatment of Alzheimer disease and other tauopathies.

Introduction

Neurofibrillary tangles (NFTs), a pathologic hallmark of Alzheimer disease (AD), are mainly composed of intracellular hyperphosphorylated and aggregated microtubule-associated protein tau (Lee et al., 2001; Ballatore et al., 2007). In addition to AD, NFTs are also present in a family of neurodegenerative diseases known as tauopathies, including frontotemporal dementia, corticobasal degeneration, Pick disease, and progressive supranuclear palsy (Lee et al., 2001). In frontotemporal dementia with parkinsonism type-17, tau is causally related to the neurodegeneration and dementia, as demonstrated by the discovery that mutations in the tau gene cause the disease (Hutton et al., 1998). These mutations may affect alternative splicing of tau mRNA, decrease the ability of tau to bind microtubules, and increase the propensity of tau to form aggregates (Dayanandan et al., 1999; Gamblin et al., 2000; Lee et al., 2001).

This work was funded by Merck Sharp & Dohme Corp., a subsidiary of Merck & Co., Inc., Kenilworth, NJ and Alectos Therapeutics Inc.
https://doi.org/10.1124/jpet.120.266122.
[S] This article has supplemental material available at jpet.aspetjournals.org.

ABBREVIATIONS: AD, Alzheimer disease; BID, twice daily; CSF, cerebrospinal fluid; GlcNAc, *N*-acetylglucosamine; HEX A/B, hexosaminidase A/B; LMA, locomotor activity; MRI, magnetic resonance imaging; MSD, MesoScale Discovery; NAGLU, *N*-acetylglucosaminidase; NFT, neurofibrillary tangle; OGA, *O*-GlcNAcase; *O*-GlcNAc, *O*-linked GlcNAc; OGT, *O*-GlcNAc transferase; PBMC, peripheral blood mononuclear cell; PET, positron emission tomography; SD, Sprague-Dawley; SPR, surface plasmon resonance; vMRI, volumetric MRI; WGA, wheat germ agglutinin.

Tau is subject to a variety of post-translational modifications, including phosphorylation, acetylation, sumoylation, isomerization, ubiquitination, nitration, and *O*-linked *N*-acetylglucosamine (*O*-GlcNAc)-ylation (Martin et al., 2011). *O*-GlcNAcylation is a noncanonical glycosylation that involves the attachment of single *O*-GlcNAc moieties to serine and threonine residues of hundreds of different proteins found in the nucleus, mitochondria, and cytosol (Yang and Qian, 2017). The dynamic cycling of this protein modification is controlled by a single pair of enzymes: *O*-GlcNAc transferase (OGT), which catalyzes the transfer of a *N*-acetylglucosamine (GlcNAc) moiety to the target serine and threonine residues, and *O*-GlcNAcase (OGA), which catalyzes the hydrolysis of this sugar modification (Hart et al., 2007). Cellular levels of *O*-GlcNAcylation are dependent on availability of the donor substrate for *O*-GlcNAcylation, UDP-GlcNAc. This donor substrate is a metabolic product of glucose through the hexosamine biosynthetic pathway, and intracellular UDP-GlcNAc levels have been shown to tightly correlate with the availability of glucose (Lefebvre et al., 2010). Therefore, *O*-GlcNAcylation may be considered as an intracellular sensor of glucose metabolism status (Gong et al., 2016).

Impaired brain glucose metabolism has been observed in multiple neurodegenerative diseases, including AD, and may play a critical role in the pathogenesis of these diseases (Hoyer, 2000; Mosconi, 2005; Butterfield and Halliwell, 2019). Functional imaging studies have consistently identified deficient glucose metabolism throughout the cortex of AD patients (Mosconi, 2005) and progression from mild cognitive impairment to AD tracks with reduction in cortical glucose metabolism (Drzezga et al., 2003; Mosconi, 2005). Consistent with these findings, *O*-GlcNAcylation levels are markedly reduced in AD brains as compared with healthy controls (Liu et al., 2004, 2009; Pinho et al., 2019). More importantly, the decrease in *O*-GlcNAcylation correlates with increased hyperphosphorylated tau levels in AD brain. This relationship suggests that reduced tau *O*-GlcNAcylation might contribute to the progression of tauopathy in AD patients (Liu et al., 2009; Gong et al., 2016).

Accumulating evidence indicates that *O*-GlcNAcylation may limit tau phosphorylation and aggregation. For example, pharmacological inhibition of OGA elevates *O*-GlcNAcylation and reduces tau phosphorylation both in vitro and in vivo (Lefebvre et al., 2003; Yuzwa et al., 2008; Hastings et al., 2017). In addition, neuronal specific deletion of OGT leads to accumulation of hyperphosphorylated tau in the brain and the spinal cord of transgenic animals (O'Donnell et al., 2004). Other than modulating tau phosphorylation, increased *O*-GlcNAcylation of tau protein has also been reported to hinder tau aggregation (Yuzwa et al., 2012, 2014). Consistent with these findings, *O*-GlcNAcylated tau is primarily detected in the less phosphorylated soluble tau species but not in hyperphosphorylated insoluble tau (Lefebvre et al., 2003; Liu et al., 2009; Graham et al., 2014; Hastings et al., 2017). In addition, reduction of protein aggregation propensity with *O*-GlcNAcylation has been demonstrated with other proteins. As an example, the polycomb protein polyhomeotic forms large aggregates in the absence of *O*-GlcNAcylation both in vitro and in vivo (Gambetta and Muller, 2014). Moreover, *O*-GlcNAc modification has been shown to block the aggregation of α-synuclein protein associated with Parkinson disease (Marotta et al., 2015; Levine et al., 2019). These findings suggest that pharmacological inhibition of OGA could increase *O*-GlcNAcylation of tau and reduce the formation of pathologic tau and could be explored as a treatment of AD and other proteinopathies provided that this mechanism does not impact the function of other essential proteins.

In this work, we characterize the in vitro and in vivo pharmacological properties of a novel and selective OGA inhibitor, MK-8719. This compound demonstrates nanomolar potency at the OGA enzyme and increases *O*-GlcNAc levels both in vitro and in vivo. In addition, MK-8719 enzyme occupancy is revealed by positron emission tomography (PET) imaging analysis. In the rTg4510 transgenic mouse model of tauopathy, MK-8719 reduces brain aggregated tau in the insoluble fraction of brain homogenates, attenuates NFT-like pathology, and ameliorates brain atrophy.

Materials and Methods

Enzyme Activity Assay. OGA enzymatic reactions were carried out in a reaction containing 50 mM NaH_2PO_4, 100 mM NaCl, and 0.1% bovine serum albumin (pH 7.0) using 2 mM 4-methylumbelliferyl *N*-acetyl-β-D-glucosaminide dihydrate (M2133; Sigma) dissolved in double distilled H_2O, as a fluorogenic substrate. The amount of purified human OGA enzyme used in the reaction was 0.7 nM. Test compound of varying concentrations was added to the enzyme prior to initiation of the reaction. The reaction was performed at room temperature in a 96-well plate and was initiated with the addition of substrate. The generation of fluorescent product, 4-methylumbelliferone, was measured every 60 seconds for 45 minutes with a Tecan Infinite M200 plate reader with excitation at 355 nM, and emission was detected at 460 nM. 4-methylumbelliferone (M1381; Sigma) was used to produce a standard curve. The slope of product production was determined for each concentration of compound tested and plotted, using standard curve-fitting algorithms for sigmoidal dose-response curves. The values for a four-parameter logistic curve fit of the data were determined. K_i values were determined using the Cheng-Prusoff equation.

Hexosaminidase A/B (HEX A/B) enzyme activity assay was performed in a similar condition as the OGA enzyme activity assay, except the amount of purified human hexosaminidase enzyme used in the reaction was 24 nM. *N*-acetylglucosaminidase (NAGLU) enzyme activity assay was also conducted in a condition similar to the OGA enzyme activity assay, except the reactions were carried out in a buffer containing 200 mM NaH_2PO_4 and 0.5% bovine serum albumin (pH 7.0) using 0.4 mM 4-methylumbelliferyl *N*-acetyl-β-D-glucosaminide dihydrate (M2133; Sigma) dissolved in double distilled H_2O as a substrate, and the amount of purified human NAGLU enzyme used in the reaction was 20 nM.

OGA Cell-Based Assay. Inhibition of cellular OGA was determined by measuring the increase of *O*-GlcNAcylated protein in PC-12 cells. Increased *O*-GlcNAcylated protein was measured by ELISA using the RL-2 antibody that binds total *O*-GlcNAcylated protein. In this assay, rat PC-12 cells were plated in 96-well plates with approximately 10,000 cells/well. Compounds to be tested were dissolved in DMSO, either 2- or 10-mM stock solution, and then diluted with DMSO and water in a two-step process using a Tecan workstation. Cells were treated with diluted compounds for 24 hours to reach a final concentration of inhibitor desired to measure a concentration-dependent response, typically, 10 3-fold dilution steps, starting at 10 μM. To prepare a cell lysate, the media from compound-treated cells were removed, and the cells were washed once with PBS and then lysed for 5 minutes at room temperature in 50 μl of PhosphoSafe reagent (Novagen Inc., Madison, WI) with protease inhibitors and phenylmethylsulfonyl fluoride. The cell lysate was collected and transferred to a new plate, which was then either coated to assay

plates directly or frozen at −80°C until used in the ELISA procedure. If desired, the total protein concentration of samples was determined using 20 μl of the sample with the BCA method.

The ELISA portion of the assay was performed in a black Maxisorp 96-well plate that was coated overnight at 4°C with 100 μl/well of the cell lysate (1:10 dilution of the lysate with PBS-containing protease inhibitors, phosphatase inhibitors, and phenylmethylsulfonyl fluoride). The day after, the wells were washed three times with 300 μl/well of wash buffer (Tris-buffered saline with 0.1% Tween 20). The wells were blocked with 100 μl/well blocking buffer (Tris-buffered saline with 0.05% Tween 20 and 2.5% bovine serum albumin). Each well was then washed two times with 300 μl/well of wash buffer. The anti–*O*-GlcNAc antibody RL-2 (Abcam, Cambridge, MA), diluted 1:1000 in blocking buffer, was added at 100 μl/well. The plate was sealed and incubated at 37°C for 2 hours with gentle shaking. The wells were then washed three times with 300 μl/well wash buffer. To detect the amount of RL-2–bound, horseradish peroxidase–conjugated goat anti-mouse secondary antibody (diluted 1:3000 in blocking buffer) was added at 100 μl/well. The plate was incubated for 60 minutes at 37°C with gentle shaking. Each well was then washed three times with 300 μl/well wash buffer. The detection reagent, 100 μl/well of Amplex Ultra RED reagent (prepared by adding 30 μl of 10 mM Amplex Ultra RED stock solution to 10 ml PBS with 18 μl 3% hydrogen peroxide, H_2O_2), was added. The detection reaction was incubated for 15 minutes at room temperature and then read with excitation at 530 nm and emission at 590 nm.

The amount of *O*-GlcNAcylated protein, as detected by the ELISA assay, was plotted for each concentration of test compound using standard curve-fitting algorithms for sigmoidal dose-response curves. The values for a four-parameter logistic curve fit of the data were determined, with the inflection point of the curve being the potency value for the test compound.

Surface Plasmon Resonance Assay. Surface plasmon resonance (SPR) analysis was performed on a Biacore T-200 instrument (Biacore; GE Healthcare, Life Sciences). Human OGA protein was captured on a series S sensor chip CM5 using amine-coupling method. The methods for immobilization and binding analysis were generated using Biacore T200 control software, version 1.0. 1-ethyl-3-(3-dimethylaminopropyl)carbodiimide hydrochloride/N-hydroxysuccinimide solutions were used to activate a carboxymethylated dextran matrix on CM5 chip surface to covalently attach human OGA protein through exposed primary amines. Usually human OGA protein was diluted to 100 μg/ml, injected over the surface of the activated CM5 chip at a flow rate of 10 μl/min for 45 seconds, and then followed by deactivation with 130 μl of 1.0 M pH 8.5 ethanolamine to achieve the immobilization level of approximately 3500 resonance units of bound protein. The binding assay was performed using the running buffer of 10 mM Hepes, pH 7.4; 150 mM NaCl; 0.005% Tween 20; 1 mM dithiothreitol; and 2% DMSO (filtered through a 0.2-μm polyethersulfone membrane). The 2X serial dilution of compound MK-8719 was made in 100% DMSO at 50X concentration followed by subsequent dilution and mixing with the running buffer. Eight different concentrations of MK-8719, from 20 to 0.078 μM in running buffer, were injected simultaneously over the immobilized and reference surfaces, and the net signal was obtained by subtracting the reference signal from the signal with immobilized enzyme. The association phase for the compound was followed for 90 seconds, and the dissociation phase was followed for 1500 seconds. Solvent corrections were run with eight different DMSO concentrations spanning the range from 1% to 3% according to the manufacturer recommendations.

Animals. This study was conducted in strict accordance with the National Research Council's Guide for the Care and Use of Laboratory Animals. The protocol was approved by the Institutional Animal Care and Use Committee Merck & Co., Inc., Kenilworth, NJ. Male Sprague-Dawley (SD) rats (Charles River) weighing 250–300 g were housed in an air-conditioned room on a 12-hour light/dark cycle with food and water available ad libitum. The rTg4510 mouse line overexpressing human 4R0N tau with P301L mutation was licensed from the Mayo Clinic and was bred and maintained at Taconic Biosciences, Hudson, NY. Briefly, the mice were generated by crossing the activator line (129S6 strain) expressing tetracycline-controlled transcriptional activator driven by the calmodulin-dependent protein kinase II-α promoter and the responder line (FVB/N strain) expressing human 4R0N tau with P301L mutation driven by tetracycline-operon responsive element as described previously (Santacruz et al., 2005). Only the F1 females with 50% 129S6 strain and 50% FVB/N strain were used in this study. The mice were housed under standard laboratory conditions of controlled temperature, humidity, and lighting (12-hour light: 12-hour dark; lights on at 6:00 AM) at Merck & Co., Inc. facility at least 1 week before undergoing behavior testing to allow acclimation.

Drug Administration. MK-8719 was prepared by Merck & Co., Inc., as described previously (Selnick et al., 2019). MK-8719 was administered either by oral gavage (5 ml/kg) or through in-diet dosing as described in Hastings et al. (2017). For oral gavage administration of MK-8719, dosing solutions were prepared by dissolving MK-8719 powder in sterile distilled water. Sterile water was administered as vehicle. After preparation, solutions were stored at 4°C and used within 24 hours. For in-diet dosing, MK-8719 was formulated in mouse chow (D01060501) by Research Diets, Inc, New Brunswick, NJ. The concentration of MK-8719 in mouse chow was calculated according to the average body weight of rTg4510 mice, average daily food intake, and dose levels. Concentration of MK-8719 in mouse chow = (dose levels × body weight)/food intake.

Brain and Peripheral Blood Mononuclear Cell *O*-GlcNAcylated Protein Assay. Male SD rats were euthanized by inhalation of CO_2 at the indicated time point after administration of vehicle or MK-8719. After euthanasia, 4 to 5 ml blood was drawn from the vena cava using an 18-gauge needle attached to a 5 ml syringe. A 4-ml CPT tube prefilled with density gradient solution and sodium citrate as anticoagulant was filled for peripheral blood mononuclear cells (PBMCs) and plasma preparation. PBMCs were prepared by generation of buffy cell layer according to the manufacturer's instructions. After centrifugation, 0.2 ml of plasma was transferred to a 96-well plate and frozen. Then 1.2 ml of the mononuclear cell layer was transferred to a 1.7-ml microcentrifuge tube. PBMC samples were centrifuged for 10 minutes at 1000*g*. Aqueous buffer was aspirated, and the cell pellets and plasma samples were frozen on dry ice and stored at −80°C.

After blood sampling, brain was harvested and dissected. All pieces were frozen on dry ice and stored at −80°C. From each animal, unilateral pieces of frontal cortex were harvested into 2-ml tubes for analysis of brain *O*-GlcNAc levels. One unilateral remnant forebrain sample was placed into a 48-well plate for measurement of compound exposures. The remaining brain structures were discarded. To each frozen brain sample, one 5-mm steel bead and 700 μl of cold PhosphoSafe homogenization buffer were added. Samples were homogenized by agitation at 30 Hz in a Qiagen TissueLyzer for 2 minutes. Samples were centrifuged at 15,000*g* for 15 minutes at 4°C. Supernatant was transferred into 96-well plates and used for protein measurements.

A sandwich immunoassay was developed to measure total *O*-GlcNAc. Biotinylated wheat germ agglutinin (WGA) (Vector Biology) at 5 μg/ml was used to coat a 96-well avidin plate [MesoScale Discovery (MSD)] in 50 ul Dulbecco's PBS buffer (Fisher) containing 5% Blocker A (MSD) and 0.2% Tween 20. After incubation for 1 hour, the plate was washed three times with 0.2% Tween 20 in PBS. Brain or PBMC homogenates in 25 μl (~100 μg protein) were added for a 3-hour incubation at room temperature before being washed three times with 0.2% Tween 20/PBS. *O*-GlcNAc antibody RL2 (1:1000 dilution; AbCam) for *O*-GlcNAc detection and sTAG goat anti-mouse antibody (MSD) were added in 50 μl 5% Blocker A and 0.2% Tween 20, and the plate was incubated at 4°C overnight. The plates were washed three times before adding 150 μl Read Buffer T (MSD) and read on a Sector 6000 Imager (MSD).

Protein Extraction and AlphaLISA-Based Immunoassays for Tau Protein. rTg4510 mice were euthanized with CO_2, and their

brains were dissected quickly. After removing the olfactory bulbs and the cerebellum, the forebrains were weighed and cut in half sagittally. The left hemi-forebrains were fixed in 10% formalin for histology, and the right hemi-forebrains were immediately frozen on dry ice and kept in −80°C for biochemical analysis. The forebrain was collected from rTg4510 mice for *O*-GlcNAc and tau protein analysis, whereas frontal cortex was harvested from SD rats to measure protein *O*-GlcNAcylation. The large size of rat frontal cortex tissue was sufficient to provide uniform dissection and pharmacodynamic measurements across animals.

To separate the soluble and insoluble tau protein fractions from rTg4510 mouse brain, hemi-forebrains were homogenized using 5-mm metal beads in a TissueLyzer (Qiagen) in 900 μl preparation buffer containing 50 mM Tris, pH 8.0; 250 mM NaCl; 5 mM KCl; 2 mM EDTA; 2 mM EGTA; Phospho-Safe extraction buffer (EMD/Novagen) plus Complete EDTA-free Protease Inhibitor Tablet (Roche); PhoStop Tablet (Roche); 2 μM Trichostatin A (Sigma-Aldrich); 5 mM nicotinamide (Sigma-Aldrich); and 1 μM PUGNAc (Sigma-Aldrich). The homogenates were centrifuged at 14,000*g* for 15 minutes to remove tissue debris. The supernatants from the first spin were then centrifuged at 100,000*g* for 30 minutes. The pellets from second spin were resuspended in preparation buffer and defined as insoluble fraction, whereas the supernatants from the second spin were defined as the soluble fraction. The insoluble fraction was used for aggregated tau and phosphorylated tau measurements. Protein concentrations were determined using the BCA assay kit (Pierce).

For the AlphaLISA-based assays, tau protein was captured by a monoclonal antibody that was biotinylated and bound to streptavidin-coated donor beads (PerkinElmer). Detection was accomplished either by a monoclonal antibody conjugated to the acceptor beads directly or by a polyclonal antibody in combination with anti-rabbit IgG-conjugated acceptor beads (PerkinElmer). Assay reactions (25 μl) were carried out in OptiPlate-384 microplates (PerkinElmer) that contained 5 μl of analyte at the specified protein concentration, 10 μl of biotinylated capture antibody (final concentration 2 nM), and 10 μl of detection antibody-conjugated acceptor beads (final concentration 20 μg/ml). After overnight incubation at 4°C, 25 μl of streptavidin donor beads were added under subdued light conditions (final concentration 40 μg/ml), and the reactions were incubated at room temperature for 60 minutes with gentle shaking. The fluorescent signal was detected on an Envision Plate Reader at 615 nm (PerkinElmer).

To detect aggregated forms of tau, biotin-HT7 was used in combination with HT7-conjugated acceptor beads. This assay detects any aggregated tau from a dimer to large aggregates of tau. The aggregated tau assay preferentially detects the 64-kD hyperphosphorylated species that is enriched in aggregated forms (Song, et al., 2015). Hyperphosphorylated tau species were determined using biotin-HT7 as the capture antibody and acceptor beads conjugated to phosphorylated tau antibodies PHF6 (Covance) or AT8 (Thermo Scientific) for detection.

Histology. Hemi-forebrains were immersion-fixed for 48 hours in 10% neutral buffered formalin at 4°C, blocked coronally into four 3-mm slabs using a brain matrix, and processed and embedded into paraffin. Immunohistochemistry was performed on 5-μm coronal sections using automated immunostainers (Ventana Medical Systems; Discovery XT) with AT8 mouse monoclonal antibody (ThermoFisher) and counterstained with hematoxylin. After coverslipping, slides were digitized using a slide scanner (Aperio ScanScopeXT; Leica), and numbers of NFT positive neurons were counted in the entorhinal cortex region using image analysis software (Aperio ImageScope) after manual determination of the region of interest.

Mouse Cerebrospinal Fluid Collection. Mice were euthanized with CO_2 and placed on the stereotaxic frame with head tilted down ~80°. The skin and muscle were carefully removed above the cisterna magna, and dura mater was exposed under a surgical microscope. A small opening on dura mater was made with the tip of a 30-G needle, and the cerebrospinal fluid (CSF) was drawn from the cisterna magna with a 20-μl pipettor. CSF samples were quickly transferred to a 500-μl eppendorf tube and frozen on dry ice. CSF total tau levels were evaluated with the AlphaLISA assay using biotin-HT7 as the capture antibody and acceptor beads conjugated to total tau antibody BT2 (Thermo Scientific) for detection.

Spontaneous Locomotor Activity. Spontaneous locomotor activity (LMA) was determined using digital activity monitors (Kinder Scientific, Poway, CA). Each apparatus consisted of a clear plexiglass box (7 × 15 inches) placed within the activity monitor. All LMA tests were performed during light cycle between 9:00 AM and 11:00 AM. A potential influence of altered circadian rhythm on LMA was not investigated in the current study. During the test, mice were free to ambulate and to rear for 30 minutes. LMA was detected by infrared photo beam breaks, and the number of beam breaks was recorded and analyzed by a computer connected to the apparatus. LMA was recorded in 10-minute segments during the 30-minute test session. Activity chambers were cleaned with a diluted alcohol solution after each test run to eliminate residual odor cues.

PET Imaging. [^{18}F]MK-8553, a novel OGA inhibitor PET ligand, has been developed as a preclinical and clinical research tool to determine target engagement and help dose selection (Li et al., 2016). In vivo occupancy studies were carried out in rTg4510 mice and SD rats from Taconic with MK-8719 to establish a drug plasma concentration–OGA enzyme occupancy relationship. [^{18}F]MK-8553 (specific activity >1000 Ci/mmol, radiochemical purity >99%) was supplied by Siemens Biomarker Research, North Wales, PA. PET imaging studies were conducted under the guiding principles of the American Physiologic Society and the Guide for the Care and Use for Laboratory Animals published by the US National Institutes of Health (NIH publication 85-23, revised 1985) and were approved by the Institutional Animal Care and Use Committee at Merck & Co., Inc.

rTg4510 mice and SD rats were anesthetized using isoflurane (4% to 5% induction, 1%–3% maintenance) through a closed-nose cone throughout the imaging session. Animals were positioned on the PET (Focus220; Siemens Medical Solution, Hoffman Estate, IL) bed side-by-side or in a mouse hotel. The brains were positioned within the center of the field of view. Body temperature was maintained at 37°C via a heating lamp control by a rectal probe connected with a temperature controller. Heart rate and SPO_2 were monitored by Pulse oximetry. MK-8719 was orally administered at 4–4.5 hours before [^{18}F]MK-8553 injection (intravenous). PET data were collected for 90 minutes starting at the time of radiotracer administration. Blood samples were taken before and at the end of the PET scan to measure drug levels. Tracer kinetic modeling utilizing a metabolite-corrected arterial input function was performed to determine OGA occupancy in rats. In mice, arterial input function cannot be used for tracer quantification because of the large volume of blood required for this approach, and an alternative approach was applied by using a Logan-plot analysis and the average cerebellum curve across all full-block scans as the nondisplaceable binding component. OGA occupancy was calculated by comparing the group average distribution volume ratio at baseline, after full block, and after drug administration. The average plasma level of MK-8719 during the PET study (rats) or the plasma level of MK-8719 at the end of the PET study (mice) was correlated to OGA enzyme occupancy.

Brain Volumetry by Volumetric Magnetic Resonance Imaging. Magnetic resonance acquisitions were performed in Charles River Discovery Research Services facility in Finland. A horizontal 11.7 T magnet with bore size 160 mm (Bruker Biospin GmbH, Karlsruhe, Germany) equipped with Bruker BGS-9-S/HP gradient set (maximum gradient strength 760 mT/m, bore 90 mm) interfaced to a Bruker BioSpec console (Bruker Biospin GmbH) was used for this study. A 72-mm volume coil was used for transmission, and mouse quadrature surface coil was used for receiving (Bruker Biospin GmbH and Rapid Biomedical GmbH, Rimpar, Germany, respectively). Three-dimensional volumetric magnetic resonance imagining (vMRI) data were acquired using a magnetization transfer–prepared 3D gradient echo sequence-fast low angle shot with the following parameters: echo

time/repetition time = 2.5/25 milliseconds, flip of 10°, acquisition/reconstruction matrix 3D 128 × 96 × 96, field of view 12.8 × 9.6 × 19.2 mm^3 with a saturation slice, and number of accumulations = 5. Magnetization transfer preparation was achieved by an 8-millisecond Gauss pulse with 768 flip and 4 kHz offset. The acquired 3D magnetic resonance images were analyzed in the coronal plane for whole brain, forebrain, cerebellar block, olfactory bulb, hippocampus, cortex, and lateral ventricle volumes using an in-house written analysis program run under an MATLAB (The MathWorks Inc., Natick, MA) environment.

Statistics. In all figures, data are presented as mean ± S.E.M. All statistics were performed with the software Prism (version 7.0; GraphPad). A P value of <0.05 was considered significant. The statistical treatment of each data set is described individually in the results.

Results

In Vitro Characterization of MK-8719. MK-8719 was initially identified as a novel OGA inhibitor with excellent brain permeability (Selnick et al., 2019). The functional activity of MK-8719 against human, rat, and dog OGA was evaluated using fluorescent intensity assays with 2 mM 4-methylumbelliferyl *N*-acetyl-β-D-glucosaminide dihydrate as a substrate. MK-8719 inhibits the activity of the purified human OGA enzyme with a K_i of 7.9 ± 0.5 nM (Fig. 1A). MK-8719 has similar in vitro potency for rat, dog, and mouse OGA enzymes, with K_i values of 9.7 ± 0.8, 12.1 ± 1.5, and 9.7 ± 0.6 nM, respectively. The cellular activity of MK-8719 against OGA was established by measuring the accumulation of *O*-GlcNAc in PC-12 cells that express rat OGA. The potency (EC_{50}) of MK-8719 was 52.7 ± 7 nM in the PC-12 cell-based *O*-GlcNAc assay (Fig. 1B). The affinity of MK-8719 for human OGA was determined using a Biacore T200 system that employs SPR technology. In this assay, MK-8719 demonstrated a K_d value of 3.1 nM. In addition, the SPR analysis also revealed the reversible nature of MK-8719 binding to OGA, with a dissociation half-life of 46 seconds.

The primary counterscreens for MK-8719 were human Hex A/B and human NAGLU assays. In vitro fluorescence intensity assays demonstrated that MK-8719 up to 1 mM had no measurable activity against HEX A/B (Supplemental Table 1). Similarly, MK-8719 at concentrations up to 1 mM did not significantly inhibit NAGLU enzyme activity (Supplemental Table 1). In addition to the targeted screens against Hex A/B and NAGLU, MK-8719 was screened for binding activity against a panel of 118 known human and animal pharmacology targets by Ricerca Biosciences to confirm selectivity of the compound. This binding assay screen did not detect any notable findings against a panel of >100 receptor and enzyme targets when MK-8719 was tested at a concentration of 10 μM (unpublished data).

Effects of OGA Inhibition on Brain and PBMC *O*-GlcNAc Levels. To determine the extent of brain OGA inhibition upon MK-8719 treatment, SD rats were orally dosed with a single administration of MK-8719 from 0.1 to 100 mg/kg. Brains were collected at 8 hours postdosing, and the brain *O*-GlcNAc levels were detected by ELISA using the RL2 antibody after WGA precipitation. MK-8719 dose-dependently increased brain *O*-GlcNAc levels up to 3.9 ± 0.18-fold at 100 mg/kg (Fig. 2A). To establish a translational pharmacodynamic biomarker using blood samples, we also investigated the *O*-GlcNAc change in PBMCs from the same cohort of rats. As expected from its high brain permeability and excellent brain-to-plasma ratio (~1.84 at 8 hours) (Selnick et al., 2019), MK-8719 increased PBMC *O*-GlcNAc levels in rats with a dose-response relationship that is similar to the increases in brain *O*-GlcNAc (Fig. 2B). Consistent with the higher exposure of MK-8719 in brain, the *O*-GlcNAc response is also more robust in brain as compared with that in PBMCs (Fig. 2B). A dose-proportional increase in MK-8719 plasma and brain exposures was also observed post–single oral administration of the compound (Fig. 2, C and D).

We investigated the temporal pattern of *O*-GlcNAc elevation in brain and PBMCs after a single administration of MK-8719 in SD rats. SD rats were orally dosed with MK-8719 at 30 mg/kg. Brain and PBMC samples were collected over a 2–8- or 8–48-hour time period postdosing for *O*-GlcNAc and drug exposure analysis. The temporal pattern of *O*-GlcNAc elevation was comparable between brain and PBMCs, with peak *O*-GlcNAc increases detected at 8–16 hours postdosing and sustained elevation observed over at least 24 hours (Fig. 3, A and B). In contrast, MK-8719 exposures peaked at 2 hours and declined over time in both brain and plasma (Fig. 3, C and D). The delayed peak *O*-GlcNAc response was likely due to continued OGT activity with the blockade of OGA activity, resulting in accumulation of *O*-GlcNAc in brain and PBMCs over time. The *O*-GlcNAc elevations were more robust in the brain (max elevation 3.9-fold at 30 mg/kg) compared with those in the PBMCs (max elevation 2.5-fold at 30 mg/kg) likely due in part to the higher exposures of MK-8719 in the brain tissue (Fig. 3, C and D).

PET Imaging in SD Rats and rTg4510 Mice. To evaluate the relationship between MK-8719 plasma concentration and brain occupancy, we developed a brain-penetrable PET tracer. [^{18}F]MK-8553 is a potent and selective inhibitor for the OGA enzyme (Li et al., 2016). Baseline PET scans with [^{18}F]MK-8553 in SD rats, rTg4510 mice, and monkeys

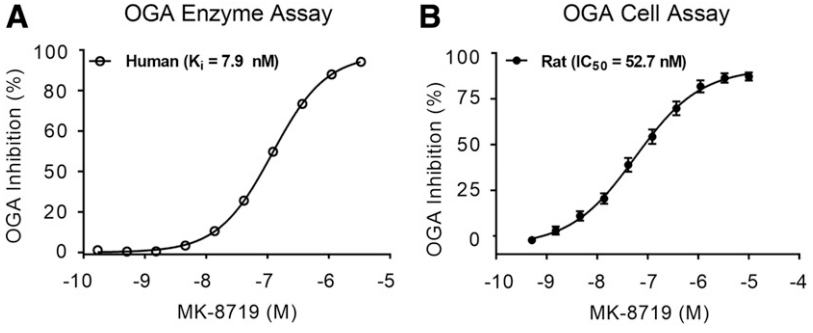

Fig. 1. Evaluation of MK-8719 in vitro potency. (A) Inhibition of human OGA enzyme activity by MK-8719. The ability of MK-8719 to functionally inhibit OGA enzyme is evaluated using a fluorescence intensity assay employing 4-methylumbelliferyl *N*-acetyl-β-D-glucosaminide dehydrate as a substrate. MK-8719 dose-dependently inhibited OGA enzyme activity (K_i = 7.9 nM). (B) Inhibition of PC12 cell-based rat OGA enzyme activity by MK-8719. Inhibition of cellular OGA activity was determined by measuring the increase of *O*-GlcNAc in PC12 cells expressing the rat OGA enzyme. MK-8719 produced a dose-dependent increase in *O*-GlcNAc in PC12 cells (IC_{50} = 52.7 nM).

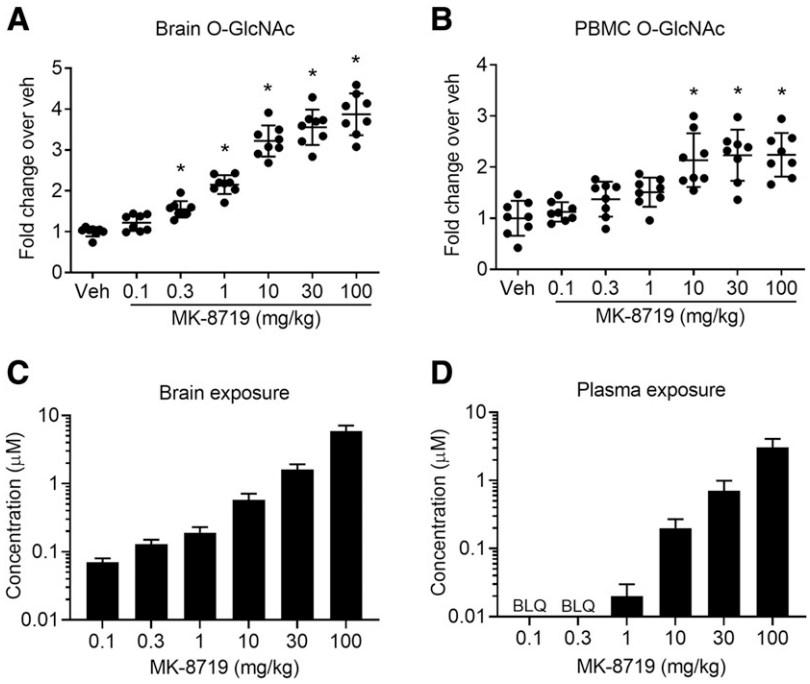

Fig. 2. Dose-dependent effects of MK-8719 treatment on brain and PBMC *O*-GlcNAc levels in SD rats. MK-8719 dose-dependently increased *O*-GlcNAc levels in both brain (A) and PBMC (B) samples at 8 hours post–single administration by oral gavage. The elevations in PBMC *O*-GlcNAc were similar to those observed in the brain. (C) Brain exposure of MK-8719 at 8 hours post–single oral administration. (D) Plasma exposure of MK-8719 at 8 hours post–single oral administration (*$P < 0.05$ compared with the vehicle groups, one-way ANOVA followed by Dunnett's post hoc test, n = 8/group). BLQ, below the limit of quantification.

revealed similar regional distribution (Li et al., 2016). The highest uptake was in striatum, and significant uptake was also observed in the hippocampus and cerebral cortex in rats (Fig. 4A) and rTg4510 mice (Fig. 5A). PET occupancy studies in animals were conducted 4–4.5 hours after oral dosing of MK-8719. [^{18}F]MK-8553-specific uptake in the striatum, hippocampus, and cerebral cortex was almost completely blocked after oral administration of OGA inhibitor MK-8719 at 10 mg/kg in SD rats (Fig. 4B) and 100 mg/kg in rTg4510 mice (Fig. 5B). The average plasma level of MK-8719 during the PET study was correlated to brain occupancy in SD rats (Fig. 4C) and rTg4510 mice (Fig. 5C). The plasma concentration–occupancy relationship for PET studies fits a typical sigmoidal equation in SD rats (Hill coefficient of 0.69 ± 0.13; Concentration required to produce 50% occupancy = 5.3 ± 1.4 nM) and rTg4510 mice (Hill coefficient of 1.55 ± 0.4; Concentration required to produce 50% occupancy = 2.6 ± 0.6 nM). In addition, the brain *O*-GlcNAc levels at the end of the study were determined and plotted against occupancy in SD rats (Fig. 4D) and rTg4510 mice (Fig. 5D). The brain

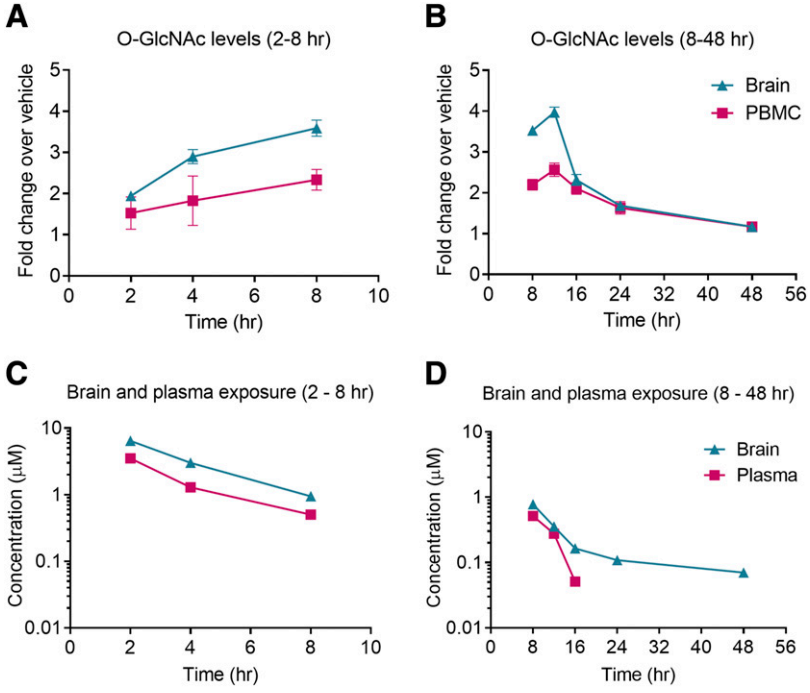

Fig. 3. Time course of brain and PBMC *O*-GlcNAc elevations after MK-8719 treatment in SD rats. (A and B) Time course of brain and PBMC *O*-GlcNAc elevation from 2 to 8 hours (A) and from 8 to 48 hours (B) after a single administration of MK-8719 at 30 mg/kg by oral gavage. (C and D) Brain and plasma exposures of MK-8719 from 2 to 8 hours (C) and from 8 to 48 hours (D) post–single oral administration of MK-8719 at 30 mg/kg (n = 8/group).

O-GlcNAc–occupancy relationship for MK-8719 in both SD rats and rTg4510 mice indicated that 80% occupancy correlated with a ~1.5-fold change in brain *O*-GlcNAc response, and OGA occupancy plateaued at levels that produced a ~2-fold brain *O*-GlcNAc elevation.

MK-8719 Attenuates Brain Tauopathies in rTg4510 Mice. rTg4510 mice, which overexpress human mutant tau (P301L) in the forebrain structures, recapitulate several key features of tau pathology in patients with tauopathies. The features include progressive age-dependent increase in hyperphosphorylated and aggregated tau species, NFTs, and brain atrophy (Santacruz et al., 2005; Song et al., 2015; Wang et al., 2018). To determine the effects of MK-8719 on brain tauopathies in rTg4510 mice, we chronically treated the mice with in-diet dosing of MK-8719 at 10, 30, and 100 mg/kg from 8 to 16 weeks of age. The compound was well-tolerated with no overt adverse effects observed in any treatment group. The animals in all groups gained weight as expected, and there were no significant differences in food intake or body weight between the treatment groups (Supplemental Fig. 1). Eight weeks of MK-8719 in-diet administration dose-dependently increased brain *O*-GlcNAc levels by 2.3-, 3.3-, and 4.7-fold at 10, 30, and 100 mg/kg, respectively (Fig. 6A). Brain samples from the baseline group were collected at 8 weeks of age without compound treatment. Eight weeks of vehicle administration from 8 to 16 weeks of age had no effect on brain *O*-GlcNAc levels ($P > 0.05$) as compared with the baseline group (Fig. 6A).

The effects of chronic MK-8719 treatment on aggregated and hyperphosphorylated tau in rTg4510 mice were evaluated by detecting various tau species in the insoluble fraction of brain homogeneous. To assess aggregated tau, we developed an HT7:HT7 AlphaLISA assay. In this assay, the total tau antibody HT7 was conjugated to both acceptor beads and donor beads. Since there is only one HT7-binding site for each tau protein, this assay only detects aggregated tau but not monomeric tau (Song et al., 2015). The assay revealed an 8.8-fold increase in aggregated tau levels between the baseline and the vehicle groups suggesting the robust progression of tau pathology in rTg4510 brain from 8 to 16 weeks of age (Fig. 6B). Eight weeks of in-diet treatment with MK-8719 dose-dependently reduced brain aggregated tau by 12.8%, 22.9%, and 26% at 10, 30, and 100 mg/kg, respectively (Fig. 6B). Significant effects of MK-8719 were observed at 30 ($P < 0.05$) and 100 mg/kg ($P < 0.01$) (Fig. 6B). To evaluate hyperphosphorylated tau, we developed HT7:PHF6 and HT7:AT8 AlphaLISA assays. In these assays, the total tau antibody HT7 was conjugated to acceptor beads and used as a capture antibody. The hyperphosphorylated tau antibodies PHF6 or AT8 were conjugated to the donor beads as detecting antibodies (Song et al., 2015). Compared with the baseline group, brain hyperphosphorylated tau levels in the vehicle group increased by ~12-fold from 8 to 16 weeks (Fig. 6, C and D). Eight weeks of in-diet dosing with MK-8719 reduced brain hyperphosphorylated PHF6 tau by 20.7%, 23.6%, and 31% at 10, 30, and 100 mg/kg, respectively (Fig. 6C), with significant reduction observed at 30 mg/kg ($P < 0.05$) and 100 mg/kg ($P < 0.01$) (Fig. 6C). Similar effects of MK-8719 were found on hyperphosphorylated AT8 tau, with 17.3%, 25%, and 30.5% reduction at 10, 30, and 100 mg/kg, respectively (Fig. 6D). In

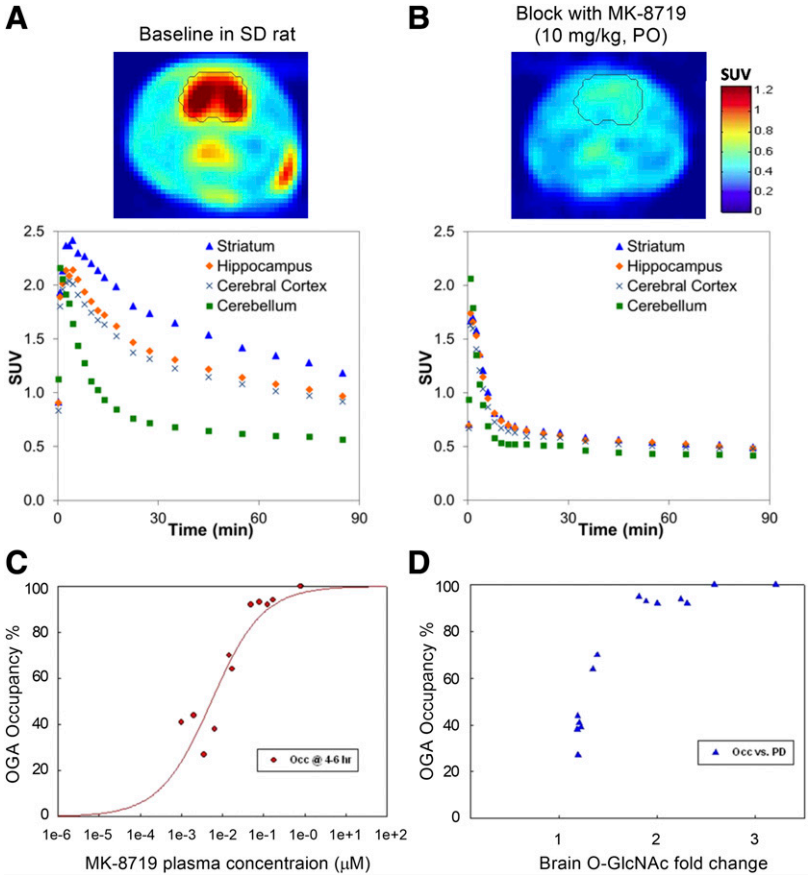

Fig. 4. MK-8719 brain occupancy in SD rats revealed by PET imaging. (A) Summed PET baseline image (upper) and time-activity curves (lower) showing the retention of [^{18}F]MK-8553 in the striatum, hippocampus,s cerebral cortex, and cerebellum of SD rats. Rat brain region is highlighted with the black circle in the coronal image. SUV, standardized uptake value. (B) [^{18}F]MK-8553–specific uptake in the striatum and other brain regions was almost completely blocked after oral administration of 10 mg/kg MK-8719 in the same animal as revealed by the summed PET image (upper) and the time-activity curves (lower). PO, by mouth. (C) Relationship between MK-8719 plasma concentration (at 6 hours post-treatment) and brain OGA occupancy. Occ, occupancy. (D) Relationship between brain *O*-GlcNAc level (at 6 hours post-treatment) and brain OGA occupancy as determined in vivo by [^{18}F]MK-8553 in SD rats. PD, pharmacodynamics.

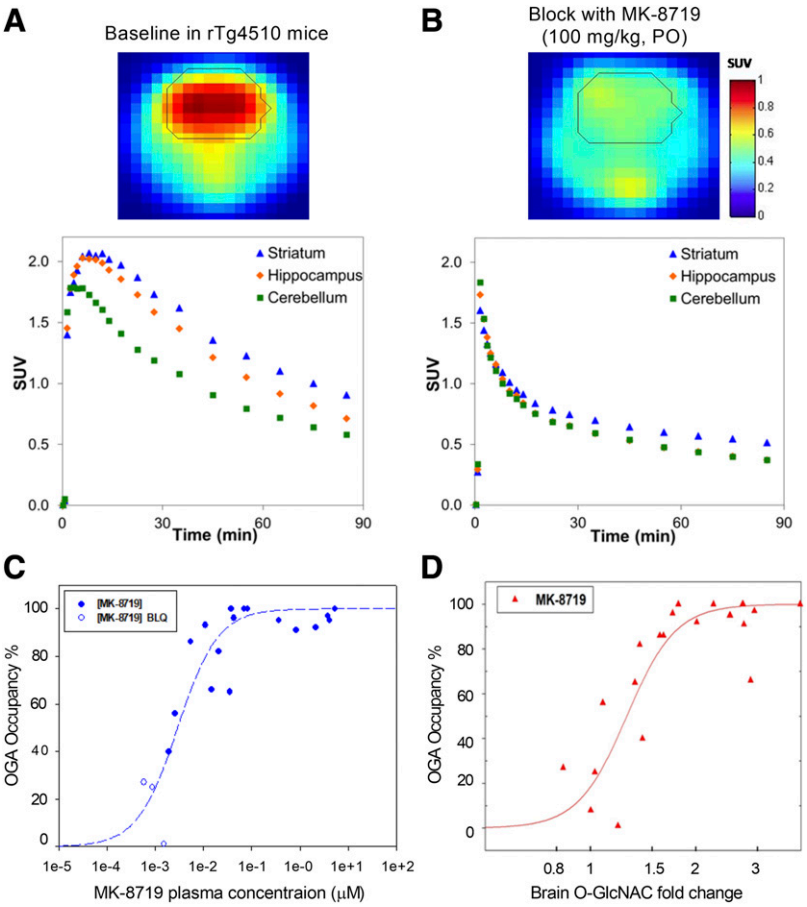

Fig. 5. MK-8719 brain occupancy in rTg4510 mice revealed by PET imaging. (A) Summed PET baseline image (upper) and time-activity curves (lower) showing the retention of [^{18}F]MK-8553 in striatum, hippocampus, and cerebellum of rTg4510 mice. Mouse brain region is highlighted with the black circle in the coronal image. SUV, standardized uptake value. (B) [^{18}F]MK-8553–specific uptake was completely blocked after oral administration of 100 mg/kg MK-8719 in the same animal as revealed by the PET image (upper) and the time-activity curves (lower). PO, by mouth. (C) Relationship between MK-8719 plasma concentration at 6 hours post-treatment and brain OGA occupancy. BLQ, below the limit of quantification. (D) Relationship between brain *O*-GlcNAc level at 6 hours post-treatment and brain OGA occupancy as determined in vivo by [^{18}F]MK-8553 in rTg4510 mice.

addition, a strong correlation between the hyperphosphorylated tau species and the aggregated tau was observed, suggesting that these endpoints may represent the same pool of pathologic tau (Fig. 6, E and F). Plasma samples were collected at the end of the 8-week in-diet dosing to determine drug concentrations. The plasma exposures of MK-8719 were 0.11 ± 0.01, 0.32 ± 0.04, and 1.05 ± 0.13 μM at 10, 30, and 100 mg/kg, respectively. These concentrations are associated with high OGA enzyme occupancy on the plasma concentration–occupancy curve in rTg4510 mice (Fig. 5C).

To better understand the effect of MK-8719 on NFT pathology in rTg4510 brain, we examined the NFT positive neurons in the entorhinal cortex using AT8 antibody immunostaining. rTg4510 mice were treated with MK-8719 at 1, 10, and 100 mg/kg in-diet from 8 to 20 weeks of age. Baseline AT8 immunostaining was determined at 8 weeks of age (Fig. 7A), and the treatment effect of MK-8719 was assessed at 20 weeks of age. Consistent with the effect of MK-8719 in reducing aggregated and hyperphosphorylated tau, NFT-like pathology was attenuated in a dose-dependent manner with significant effect observed at 100 mg/kg ($P < 0.05$) (Fig. 7, B–D).

Effects of MK-8719 Treatment on CSF Total Tau and Hyper-Locomotor Activity. CSF total tau levels are elevated in AD patients, which may reflect axonal degeneration and tau pathology observed in AD brain (Hansson et al., 2006). In addition, age-dependent increases in CSF total tau levels have been reported in AD animal models, including rTg4510 mice (Barten et al., 2011; Song et al., 2015). We asked whether OGA inhibition with MK-8719 can reduce CSF total tau in parallel to the attenuation of tau pathology in rTg4510 mice. To address this question, rTg4510 mice were orally dosed with either vehicle or MK-8719 at 50 and 100 mg/kg [twice daily (BID)] from 8 to 20 weeks of age, and CSF samples were collected at 20 weeks of age for total tau analysis. MK-8719 dose-dependently reduced CSF total tau, with significant effects observed at 100 mg/kg ($P < 0.05$) (Fig. 8A).

Age-dependent increase in LMA in rTg4510 mice is a unique behavioral phenotype that strongly correlates with brain tau pathology (Wang et al., 2018). Therefore, LMA can serve as a behavioral pharmacodynamic measurement of MK-8719 activity in rTg4510 mice, although it may not translate to efficacy of this mechanism in AD patients. To determine whether MK-8719 treatment can ameliorate the progression of hyperactivity, the same cohort of rTg4510 mice used for the CSF total tau study were evaluated for locomotor function at 8, 12, 16, and 20 weeks of age. As compared with baseline LMA at 8 weeks of age, rTg4510 mice in the vehicle group showed 2.0-, 2.5-, and 2.6-fold increase in LMA at 12, 16, and 20 weeks of age, respectively (Fig. 8B). MK-8719 at 100 mg/kg (BID) significantly attenuated the progression of hyperactivity at 16 ($P < 0.05$) and 20 ($P < 0.05$) weeks of age as compared with the vehicle group (Fig. 8B).

Chronic MK-8719 Treatment Ameliorates Brain Atrophy in rTg4510 Mice. rTg4510 mice exhibit severe neurodegeneration in forebrain structures, the brain regions that overexpress human mutant tau (Santacruz et al., 2005; Wang et al., 2018). To determine whether MK-8719 can attenuate brain atrophy in rTg4510 mice, we orally dosed the mice with

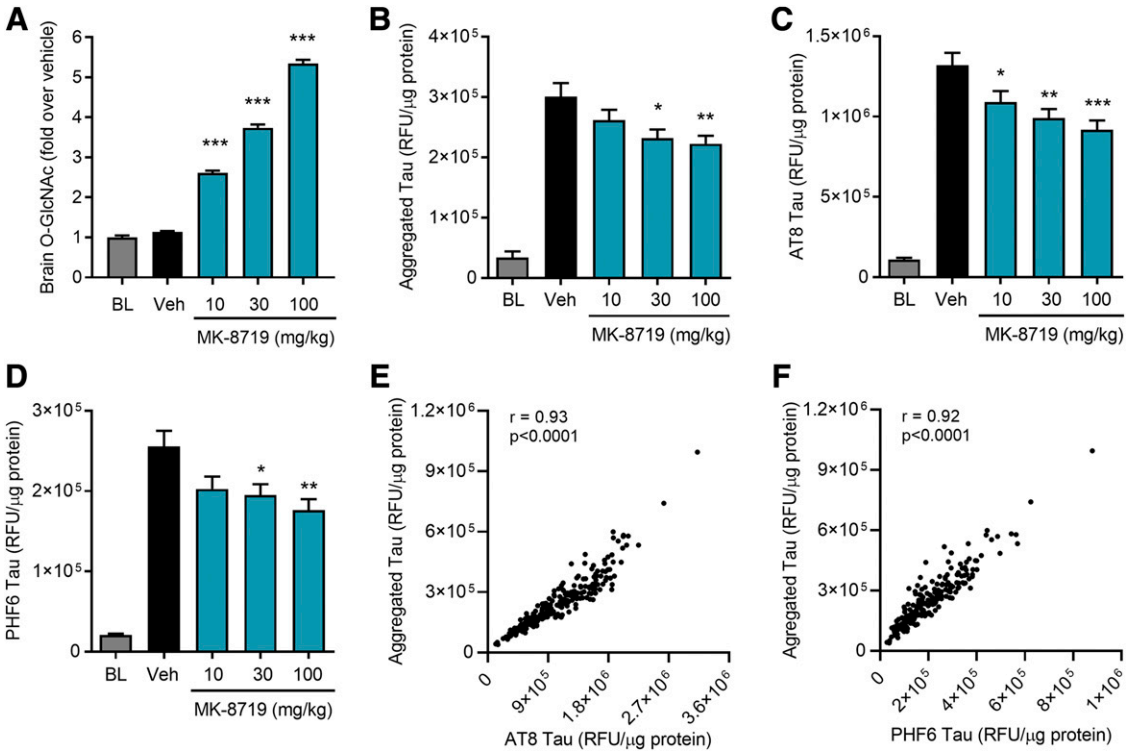

Fig. 6. Effects of chronic MK-8719 treatment on brain *O*-GlcNAc and pathologic tau species in rTg4510 mice. MK-8719 at 10, 30, and 100 mg/kg or vehicle was administered in-diet to rTg4510 mice from 8 to 16 weeks of age. Baseline samples were collected at 8 weeks of age without any treatment. (A) MK-8719 increased brain *O*-GlcNAc level detected by ELISA using the RL2 antibody after WGA precipitation. (B–D) MK-8719 reduced aggregated tau detected by HT7/HT7 AlphaLISA (B) and decreased hyperphosphorylated tau recognized by PHF6 (C) and AT8 (D) antibodies. RFU, relative fluorescence unit. (*$P < 0.05$; **$P < 0.01$; ***$P < 0.001$ compared with the vehicle group, $n = 56$/group, one-way ANOVA followed by Dunnett's test compared with the vehicle). (E and F) Correlations between levels of aggregated tau (HT7/HT7), AT8 tau, and PHF6 tau were determined using data from all vehicle- and MK-8719–treated animals ($n = 226$). Veh, vehicle.

vehicle or MK-8719 at 100 mg/kg (BID) from 8 to 32 weeks of age and periodically examined cortical, hippocampal, and lateral ventricle volumes with longitudinal vMRI. From 16 to 32 weeks of age, cortical and hippocampal volumes declined, whereas lateral ventricle volume increased in rTg4510 mice (Fig. 9, A–C). MK-8719 significantly attenuated cortical volume decline at 24 ($P < 0.05$) and 32 weeks of age ($P < 0.05$) (Fig. 9A). In addition, hippocampal volume decline was

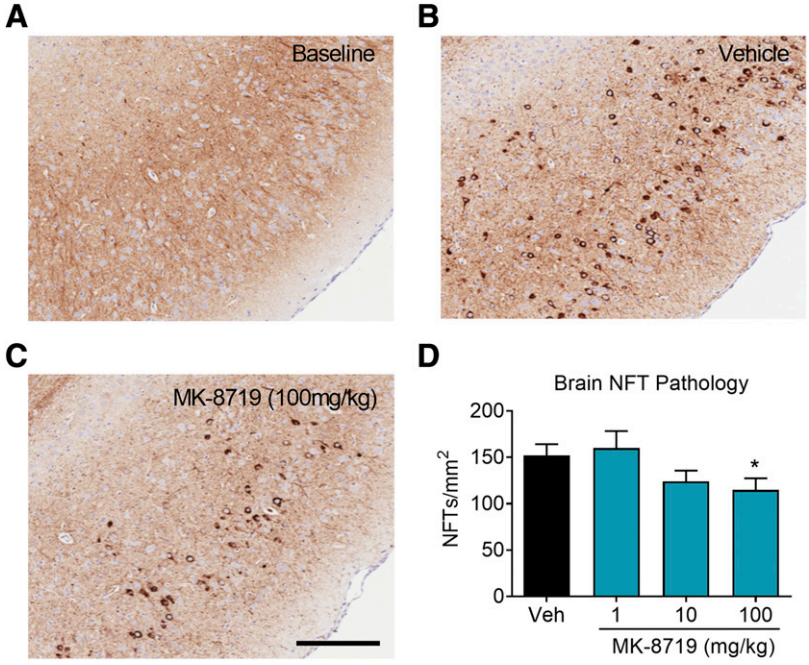

Fig. 7. Effects of MK-8719 on NFT-like pathology in the entorhinal cortex of rTg4510 mice. rTg4510 mice were administered MK-8719 (1, 10, and 100 mg/kg) or vehicle via in-diet dosing from 8 to 20 weeks of age. Baseline levels of AT8 immunoreactivity were evaluated in 8-week-old animals, and the effects of MK-8719 were determined in 20-week-old rTg4510 mice. (A–C) Representative images of NFT-like pathology in the entorhinal cortex of rTg4510 mice determined by AT8 immunostaining. Scale bar, 100 μm. (D) MK-8719 reduced NFTs in a dose-dependent manner (*$P < 0.05$, $n = 25$/group, one-way ANOVA followed by Dunnett's test compared with the vehicle). Veh, vehicle.

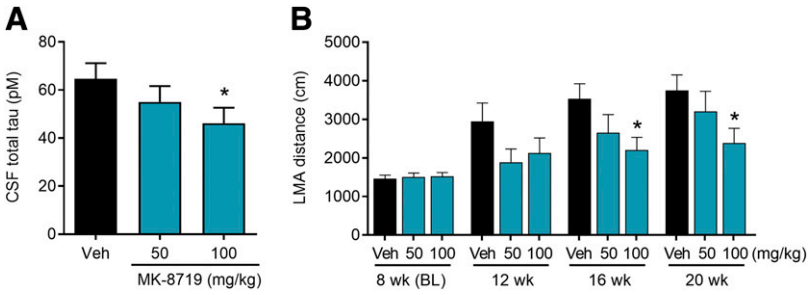

Fig. 8. Effects of MK-8719 treatment on CSF total tau and LMA in rTg4510 mice. (A) MK-8719 dose-dependently reduced CSF total tau levels in rTg4510 mice. rTg4510 mice were orally dosed with either vehicle or MK-8719 at 50 and 100 mg/kg, BID from 8 to 20 weeks of age. CSF total tau levels were determined at 20 weeks of age (n = 25 mice/group, $^*P < 0.05$, one-way ANOVA followed by Dunnett's test compared with the vehicle group). (B) MK-8719 treatment ameliorated the progression of hyper-locomotor activity in rTg4510 mice. LMA was evaluated at 8, 12, 16, and 20 weeks of age, and significant effects of MK-8719 were observed at 16 and 20 weeks of age (n = 25 mice/group, $^*P < 0.05$, one-way ANOVA followed by Dunnett's test compared with the vehicle group). Veh, vehicle.

significantly ameliorated with MK-8719 treatment at 32 weeks of age ($P < 0.05$) (Fig. 9B). Significant reduction in lateral ventricle enlargement was detected at 24 weeks of age ($P < 0.05$) (Fig. 9C), whereas a trend toward reduction in lateral ventricle volume was observed at 32 weeks of age in MK-8719–treated mice (Fig. 9C). Forebrain weight was examined at the end of the study when the mice were 32 weeks of age. MK-8719 treatment from 8 to 32 weeks of age significantly slowed down brain atrophy in rTg4510 mice ($P < 0.01$) (Fig. 9D).

Discussion

The current study provides an extensive characterization of the effects of OGA inhibition on tauopathy in preclinical models by using MK-8719, a highly selective and potent inhibitor of OGA enzyme with similar potency across multiple species. In both a PC12 cell-based assay and SD rat brain, MK-8719 dose-dependently increased *O*-GlcNAc levels. In the rTg4510 mouse model of tauopathy, MK-8719 attenuated aggregated and hyperphosphorylated tau species in the insoluble fraction of the brain homogenates, reduced CSF total tau and brain NFT-like pathology, and ameliorated brain atrophy. More importantly, the plasma concentration–OGA occupancy relationship was established for MK-8179 in both SD rats and rTg4510 mice with the OGA PET tracer [^{18}F]MK-8553.

Determining the level of enzyme occupancy necessary for efficacy provides a noninvasive translational biomarker ideal for assessing the dose range required to engage targeted enzyme in preclinical and clinical studies. The PET imaging

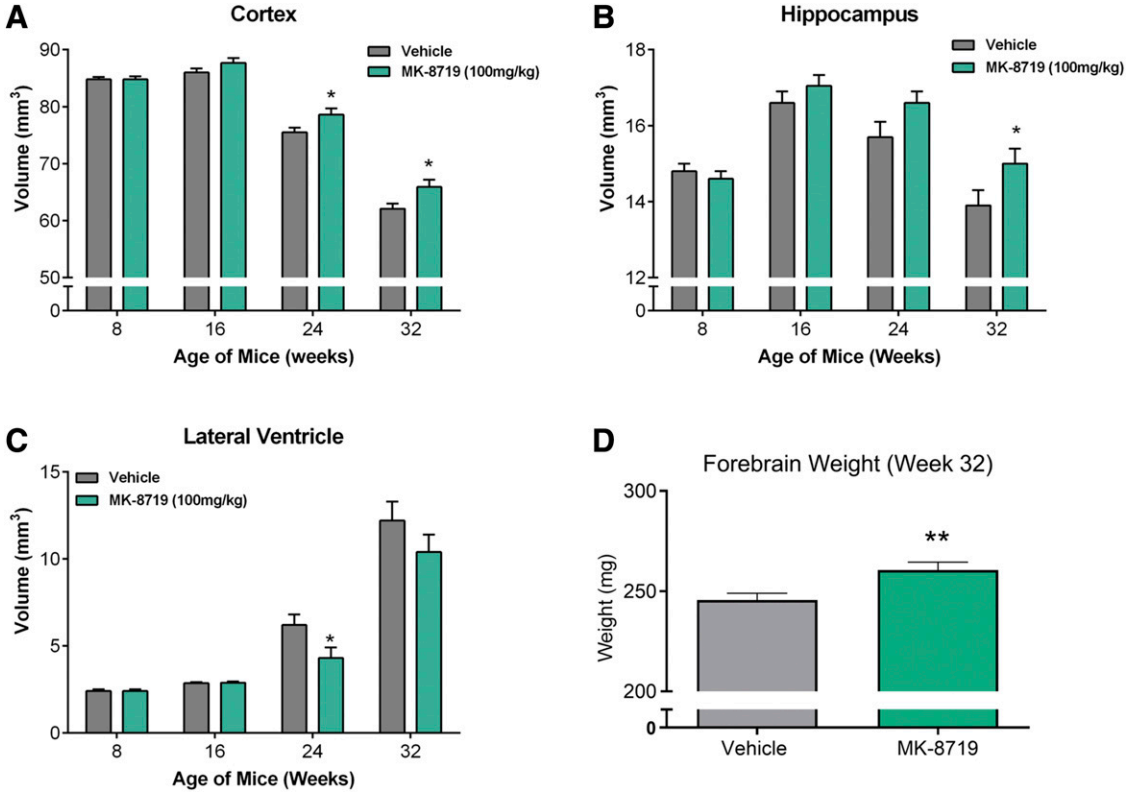

Fig. 9. Effects of MK-8719 treatment on brain volume and brain weight in rTg4510 mice. (A–C) Oral administration of MK-8719 (100 mg/kg, BID) significantly attenuated brain degeneration. rTg4510 mice were treated with vehicle or MK-8719 from 8 to 32 weeks of age. Cortex, hippocampus, and lateral ventricle volume was measured using vMRI at 8, 16, 24 and 32 weeks of age (n = 21/group; $^*P < 0.05$, t test compared with vehicle group). (D) MK-8719 (100 mg/kg, BID) significantly attenuated forebrain weight loss in rTg4510 mice. Forebrain weight of vehicle- and MK-8719–treated mice were determined at 32 weeks of age (n = 21/group; $^*P < 0.05$, t test compared with vehicle group).

studies revealed that high degree of enzyme occupancy is required to drive brain *O*-GlcNAc increases in SD rats and rTg4510 mice. As demonstrated by the relationship between MK-8719 brain *O*-GlcNAc and brain occupancy, 80% enzyme occupancy correlated with only ~1.5-fold elevation in brain *O*-GlcNAc, and near-maximal occupancy is required to achieve >3-fold brain *O*-GlcNAc increase. This is consistent with our previous observations in which 80% knockdown of OGA protein in the OGA-inducible knockdown mice was only associated with 1.4-fold increase in brain *O*-GlcNAc, and 500 mg/kg dose of the potent OGA inhibitor Thiamet-G was needed to produce >3-fold brain *O*-GlcNAc elevation after a single oral administration (Hastings et al., 2017). Indeed, a 500-mg/kg dose of Thiamet-G was typically administered in tau transgenic models to evaluate the effects of OGA inhibition on tauopathy (Yuzwa et al., 2012; Borghgraef et al., 2013; Graham et al., 2014; Hastings et al., 2017; Wang et al., 2018). To determine the level of enzyme occupancy required for reducing aggregated and hyperphosphorylated tau in rTg4510 brain, we assessed MK-8179 at 10, 30, and 100 mg/kg, the dose levels that are associated with high enzyme occupancy on the plasma concentration–occupancy curve in rTg4510 mice. At such high occupancy levels, MK-8719 was still able to demonstrate clear dose-dependent effects on brain *O*-GlcNAc elevation and pathologic tau reduction. In addition, significant effects of MK-8719 on brain NFT-like pathology, CSF total tau level, and hyper-locomotor activity were only observed at 100-mg/kg dose but not at lower doses, suggesting that extremely high enzyme occupancy is critical to *O*-GlcNAc change and attenuation of tauopathy in vivo. [^{18}F]MK-8553 can be used as a valuable clinical tool to establish MK-8719 plasma concentration–occupancy relationship for translational modeling.

Several mechanisms have been proposed to elucidate the beneficial effects of OGA inhibition in animal models of tauopathy, including reduction of tau phosphorylation upon acute treatment with OGA inhibitors (Yuzwa et al., 2008; Yu et al., 2012; Graham et al., 2014), limiting the formation of tau aggregates (Yuzwa et al., 2012; Hastings et al., 2017) and enhancement of autophagy through an mechanistic target of rapamycin–independent pathway (Zhu et al., 2018). By employing a novel *O*-GlcNAc detection method involving "click" *N*-acetylgalactosamine derivatization coupled with tetramethylrhodamine labeling, we have previously demonstrated *O*-GlcNAc modification of tau after chronic treatment of rTg4510 mice with Thiamet-G, which is structurally similar to MK-8719 (Hastings et al., 2017). One of the most consistent findings from the tau transgenic models chronically treated with the OGA inhibitor Thiamet-G is the reduction of aggregated and hyperphosphorylated tau species in the insoluble fraction of brain homogenates (Yuzwa et al., 2012; Graham et al., 2014; Hastings et al., 2017; Wang et al., 2018). In addition, it has been shown that chronic OGA inhibition in tau transgenic models has no effect on the phosphorylation status of soluble nonpathologic tau species. As such, *O*-GlcNAcylation may not directly regulate the phosphorylation of tau (Yuzwa et al., 2012; Graham et al., 2014). Moreover, *O*-GlcNAcylated tau was primarily detected in the soluble nonpathologic tau species but not in the insoluble aggregated tau, suggesting that addition of polar *O*-GlcNAc moieties may render tau less prone to aggregation (Graham et al., 2014; Hastings et al., 2017). Consistent with these findings, the current study demonstrated reduction in aggregated tau and several phosphorylated tau species in the insoluble fraction of rTg4510 brain upon chronic MK-8719 treatment. Importantly, the phosphorylated tau species closely correlated with the aggregated tau, indicating that these endpoints may represent the same pool of aggregated tau that was attenuated by OGA inhibition. Overall, these data support the hypothesis that *O*-GlcNAc modification of tau reduces the propensity of tau to form aggregates and therefore ameliorate tauopathy.

Magnetic resonance imaging (MRI)-based measures of brain atrophy are regarded as valuable markers of neurodegenerative diseases and are increasingly used as outcome measures in clinical studies of disease-modifying therapies (Frisoni et al., 2010). In AD patients, vMRI studies have shown that the rates of brain atrophy in several structural measures, including hippocampus, entorhinal cortex, whole brain, and ventricle enlargement, correlate closely with changes in cognitive performance (Fox et al., 1999; Jack et al., 2004; Thompson et al., 2004; Schott et al., 2008; Sluimer et al., 2010). rTg4510 mice develop severe age-dependent atrophy and neuron loss in forebrain structures, the regions that overexpress human mutant P301L tau under the control of the calmodulin-dependent protein kinase II promoter (Ramsden et al., 2005; Santacruz et al., 2005; Yang et al., 2011; Wang et al., 2018). The current vMRI study shows that, between 16 and 32 weeks of age, the cortical and hippocampal volume of rTg4510 mice decreased by 27.8% and 16.8%, respectively, whereas lateral ventricle volume increased by 3.2-fold. Importantly, chronic OGA inhibition with MK-8719 can ameliorate brain atrophy in multiple forebrain regions, suggesting that vMRI may serve as translational biomarker to evaluate the efficacy of OGA inhibitors in clinical settings.

In summary, the present study characterizes the robust in vitro and in vivo pharmacological profiles of OGA inhibition. Significant increases in brain and PBMC *O*-GlcNAc were detected in response to MK-8719 administration in rodent. With the OGA PET tracer [^{18}F]MK-8553, we were able to demonstrate that high degree of enzyme occupancy is required to drive brain *O*-GlcNAc elevation and ameliorate brain tauopathy. The focus of the current studies was to evaluate the effects of MK-8719 on the target protein tau related to AD. However, OGA inhibition influences *O*-GlcNAc modification on hundreds of proteins. Therefore, it will be important to understand the physiologic and toxicological consequences of prolonged elevation of *O*-GlcNAcylated proteins throughout the proteome. These findings provide a rationale for testing the hypothesis that OGA inhibition may be a promising therapeutic strategy for treatment of tauopathies.

Authorship Contributions

Participated in research design: Wang, Li, Marcus, Pearson, K. Smith, Lee, Chen, Hostetler, Sur, Zhang, Schachter, Hess, Selnick, Vocadlo, McEachern, Uslaner, Duffy, S.M. Smith.

Conducted experiments: Wang, Li, Marcus, Pearson, Song, K. Smith, Terracina, Lee, Hong, Lu, Hyde, Chen, Kinsley, Melchor, Meng.

Performed data analysis: Wang, Li, Marcus, Pearson, Song, K. Smith, Terracina, Lee, Hong, Lu, Hyde, Chen, Melchor, Rubins, Zhang, Hess, S.M. Smith.

Wrote or contributed to the writing of the manuscript: Wang, Li, Marcus, Sur, Zhang, Schachter, Hess, Selnick, Vocadlo, McEachern, Uslaner, Duffy, S.M. Smith.

References

Ballatore C, Lee VM, and Trojanowski JQ (2007) Tau-mediated neurodegeneration in Alzheimer's disease and related disorders. *Nat Rev Neurosci* **8**:663–672.

Barten DM, Cadelina GW, Hoque N, DeCarr LB, Guss VL, Yang L, Sankaranarayanan S, Wes PD, Flynn ME, Meredith JE, et al. (2011) Tau transgenic mice as models for cerebrospinal fluid tau biomarkers. *J Alzheimers Dis* **24** (Suppl 2): 127–141.

Borghgraef P, Menuet C, Theunis C, Louis JV, Devijver H, Maurin H, Smet-Nocca C, Lippens G, Hilaire G, Gijsen H, et al. (2013) Increasing brain protein O-GlcNAcylation mitigates breathing defects and mortality of Tau.P301L mice. *PLoS One* **8**: e84442.

Butterfield DA and Halliwell B (2019) Oxidative stress, dysfunctional glucose metabolism and Alzheimer disease. *Nat Rev Neurosci* **20**:148–160.

Dayanandan R, Van Slegtenhorst M, Mack TG, Ko L, Yen SH, Leroy K, Brion JP, Anderton BH, Hutton M, and Lovestone S (1999) Mutations in tau reduce its microtubule binding properties in intact cells and affect its phosphorylation. *FEBS Lett* **446**:228–232.

Drzezga A, Lautenschlager N, Siebner H, Riemenschneider M, Willoch F, Minoshima S, Schwaiger M, and Kurz A (2003) Cerebral metabolic changes accompanying conversion of mild cognitive impairment into Alzheimer's disease: a PET follow-up study. *Eur J Nucl Med Mol Imaging* **30**:1104–1113.

Fox NC, Scahill RI, Crum WR, and Rossor MN (1999) Correlation between rates of brain atrophy and cognitive decline in AD. *Neurology* **52**:1687–1689.

Frisoni GB, Fox NC, Jack CR Jr., Scheltens P, and Thompson PM (2010) The clinical use of structural MRI in Alzheimer disease. *Nat Rev Neurol* **6**:67–77.

Gambetta MC and Müller J (2014) O-GlcNAcylation prevents aggregation of the Polycomb group repressor polyhomeotic. *Dev Cell* **31**:629–639.

Gamblin TC, King ME, Dawson H, Vitek MP, Kuret J, Berry RW, and Binder LI (2000) In vitro polymerization of tau protein monitored by laser light scattering: method and application to the study of FTDP-17 mutants. *Biochemistry* **39**: 6136–6144.

Gong CX, Liu F, and Iqbal K (2016) O-GlcNAcylation: a regulator of tau pathology and neurodegeneration. *Alzheimers Dement* **12**:1078–1089.

Graham DL, Gray AJ, Joyce JA, Yu D, O'Moore J, Carlson GA, Shearman MS, Dellovade TL, and Hering H (2014) Increased O-GlcNAcylation reduces pathological tau without affecting its normal phosphorylation in a mouse model of tauopathy. *Neuropharmacology* **79**:307–313.

Hansson O, Zetterberg H, Buchhave P, Londos E, Blennow K, and Minthon L (2006) Association between CSF biomarkers and incipient Alzheimer's disease in patients with mild cognitive impairment: a follow-up study. *Lancet Neurol* **5**:228–234.

Hart GW, Housley MP, and Slawson C (2007) Cycling of O-linked beta-N-acetylglucosamine on nucleocytoplasmic proteins. *Nature* **446**:1017–1022.

Hastings NB, Wang X, Song L, Butts BD, Grotz D, Hargreaves R, Fred Hess J, Hong KK, Huang CR, Hyde L, et al. (2017) Inhibition of O-GlcNAcase leads to elevation of O-GlcNAc tau and reduction of tauopathy and cerebrospinal fluid tau in rTg4510 mice. *Mol Neurodegener* **12**:39.

Hoyer S (2000) Brain glucose and energy metabolism abnormalities in sporadic Alzheimer disease. Causes and consequences: an update. *Exp Gerontol* **35**: 1363–1372.

Hutton M, Lendon CL, Rizzu P, Baker M, Froelich S, Houlden H, Pickering-Brown S, Chakraverty S, Isaacs A, Grover A, et al. (1998) Association of missense and 5′-splice-site mutations in tau with the inherited dementia FTDP-17. *Nature* **393**: 702–705.

Jack CR Jr., Shiung MM, Gunter JL, O'Brien PC, Weigand SD, Knopman DS, Boeve BF, Ivnik RJ, Smith GE, Cha RH, et al. (2004) Comparison of different MRI brain atrophy rate measures with clinical disease progression in AD. *Neurology* **62**: 591–600.

Lee VM, Goedert M, and Trojanowski JQ (2001) Neurodegenerative tauopathies. *Annu Rev Neurosci* **24**:1121–1159.

Lefebvre T, Dehennaut V, Guinez C, Olivier S, Drougat L, Mir AM, Mortuaire M, Vercoutter-Edouart AS, and Michalski JC (2010) Dysregulation of the nutrient/stress sensor O-GlcNAcylation is involved in the etiology of cardiovascular disorders, type-2 diabetes and Alzheimer's disease. *Biochim Biophys Acta* **1800**:67–79.

Lefebvre T, Ferreira S, Dupont-Wallois L, Bussière T, Dupire MJ, Delacourte A, Michalski JC, and Caillet-Boudin ML (2003) Evidence of a balance between phosphorylation and O-GlcNAc glycosylation of Tau proteins--a role in nuclear localization. *Biochim Biophys Acta* **1619**:167–176.

Levine PM, Galesic A, Balana AT, Mahul-Mellier AL, Navarro MX, De Leon CA, Lashuel HA, and Pratt MR (2019) α-Synuclein O-GlcNAcylation alters aggregation and toxicity, revealing certain residues as potential inhibitors of Parkinson's disease. *Proc Natl Acad Sci USA* **116**:1511–1519.

Li WP, Salinas C, Riffel K, Miller P, Zeng ZZ, Lohith T, Selnick HG, Purcell M, Holahan M, Meng XJ, et al. (2016) The discovery and characterization of [^{18}F]MK-8553, a novel PET tracer for imaging O-GlcNAcase (OGA), in *International Symposium on Function NeuroReceptor Mapping of the Living Brain (NRM2016)*; Boston, MA.

Liu F, Iqbal K, Grundke-Iqbal I, Hart GW, and Gong CX (2004) O-GlcNAcylation regulates phosphorylation of tau: a mechanism involved in Alzheimer's disease. *Proc Natl Acad Sci USA* **101**:10804–10809.

Liu F, Shi J, Tanimukai H, Gu J, Gu J, Grundke-Iqbal I, Iqbal K, and Gong CX (2009) Reduced O-GlcNAcylation links lower brain glucose metabolism and tau pathology in Alzheimer's disease. *Brain* **132**:1820–1832.

Marotta NP, Lin YH, Lewis YE, Ambroso MR, Zaro BW, Roth MT, Arnold DB, Langen R, and Pratt MR (2015) O-GlcNAc modification blocks the aggregation and toxicity of the protein α-synuclein associated with Parkinson's disease. *Nat Chem* **7**:913–920.

Martin L, Latypova X, and Terro F (2011) Post-translational modifications of tau protein: implications for Alzheimer's disease. *Neurochem Int* **58**:458–471.

Mosconi L (2005) Brain glucose metabolism in the early and specific diagnosis of Alzheimer's disease. FDG-PET studies in MCI and AD. *Eur J Nucl Med Mol Imaging* **32**:486–510.

O'Donnell N, Zachara NE, Hart GW, and Marth JD (2004) Ogt-dependent X-chromosome-linked protein glycosylation is a requisite modification in somatic cell function and embryo viability. *Mol Cell Biol* **24**:1680–1690.

Pinho TS, Correia SC, Perry G, Ambrósio AF, and Moreira PI (2019) Diminished O-GlcNAcylation in Alzheimer's disease is strongly correlated with mitochondrial anomalies. *Biochim Biophys Acta Mol Basis Dis* **1865**:2048–2059.

Ramsden M, Kotilinek L, Forster C, Paulson J, McGowan E, SantaCruz K, Guimaraes A, Yue M, Lewis J, Carlson G, et al. (2005) Age-dependent neurofibrillary tangle formation, neuron loss, and memory impairment in a mouse model of human tauopathy (P301L). *J Neurosci* **25**:10637–10647.

Santacruz K, Lewis J, Spires T, Paulson J, Kotilinek L, Ingelsson M, Guimaraes A, DeTure M, Ramsden M, McGowan E, et al. (2005) Tau suppression in a neurodegenerative mouse model improves memory function. *Science* **309**:476–481.

Schott JM, Crutch SJ, Frost C, Warrington EK, Rossor MN, and Fox NC (2008) Neuropsychological correlates of whole brain atrophy in Alzheimer's disease. *Neuropsychologia* **46**:1732–1737.

Selnick HG, Hess JF, Tang C, Liu K, Schachter JB, Ballard JE, Marcus J, Klein DJ, Wang X, Pearson M, et al. (2019) Discovery of MK-8719, a potent O-GlcNAcase inhibitor as a potential treatment for tauopathies. *J Med Chem* **62**:10062–10097.

Sluimer JD, Bouwman FH, Vrenken H, Blankenstein MA, Barkhof F, van der Flier WM, and Scheltens P (2010) Whole-brain atrophy rate and CSF biomarker levels in MCI and AD: a longitudinal study. *Neurobiol Aging* **31**:758–764.

Song L, Lu SX, Ouyang X, Melchor J, Lee J, Terracina G, Wang X, Hyde L, Hess JF, Parker EM, et al. (2015) Analysis of tau post-translational modifications in rTg4510 mice, a model of tau pathology. *Mol Neurodegener* **10**:14.

Thompson PM, Hayashi KM, Sowell ER, Gogtay N, Giedd JN, Rapoport JL, de Zubicaray GI, Janke AL, Rose SE, Semple J, et al. (2004) Mapping cortical change in Alzheimer's disease, brain development, and schizophrenia. *Neuroimage* **23** (Suppl 1):S2–S18.

Wang X, Smith K, Pearson M, Hughes A, Cosden ML, Marcus J, Hess JF, Savage MJ, Rosahl T, Smith SM, et al. (2018) Early intervention of tau pathology prevents behavioral changes in the rTg4510 mouse model of tauopathy. *PLoS One* **13**: e0195486.

Yang D, Xie Z, Stephenson D, Morton D, Hicks CD, Brown TM, Sriram R, O'Neill S, Raunig D, and Bocan T (2011) Volumetric MRI and MRS provide sensitive measures of Alzheimer's disease neuropathology in inducible Tau transgenic mice (rTg4510). *Neuroimage* **54**:2652–2658.

Yang X and Qian K (2017) Protein O-GlcNAcylation: emerging mechanisms and functions. *Nat Rev Mol Cell Biol* **18**:452–465.

Yu Y, Zhang L, Li X, Run X, Liang Z, Li Y, Liu Y, Lee MH, Grundke-Iqbal I, Iqbal K, et al. (2012) Differential effects of an O-GlcNAcase inhibitor on tau phosphorylation. *PLoS One* **7**:e35277.

Yuzwa SA, Cheung AH, Okon M, McIntosh LP, and Vocadlo DJ (2014) O-GlcNAc modification of tau directly inhibits its aggregation without perturbing the conformational properties of tau monomers. *J Mol Biol* **426**:1736–1752.

Yuzwa SA, Macauley MS, Heinonen JE, Shan X, Dennis RJ, He Y, Whitworth GE, Stubbs KA, McEachern EJ, Davies GJ, et al. (2008) A potent mechanism-inspired O-GlcNAcase inhibitor that blocks phosphorylation of tau in vivo. *Nat Chem Biol* **4**: 483–490.

Yuzwa SA, Shan X, Macauley MS, Clark T, Skorobogatko Y, Vosseller K, and Vocadlo DJ (2012) Increasing O-GlcNAc slows neurodegeneration and stabilizes tau against aggregation. *Nat Chem Biol* **8**:393–399.

Zhu Y, Shan X, Safarpour F, Erro Go N, Li N, Shan A, Huang MC, Deen M, Holicek V, Ashmus R, et al. (2018) Pharmacological inhibition of O-GlcNAcase enhances autophagy in brain through an mTOR-independent pathway. *ACS Chem Neurosci* **9**:1366–1379.

Address correspondence to: Dr. Xiaohai Wang, MRL, Merck & Co., Inc., 770 Sumneytown Pike, WP14-3393, West Point, PA 19486. E-mail: xiaohai_wang@merck.com

Title page for supplemental data

MK-8719, a novel and selective O-GlcNAcase inhibitor that reduces the formation of pathological tau and ameliorates neurodegeneration in a mouse model of tauopathy

Xiaohai Wang, Wenping Li, Jacob Marcus, Michelle Pearson, Lixin Song, Karen Smith, Giuseppe Terracina, Julie Lee, Kwok-Lam Karen Hong, Sherry X. Lu, Lynn Hyde, Shu-Cheng Chen, David Kinsley, Jerry P. Melchor, Daniel J. Rubins, Xiangjun Meng, Eric Hostetler, Cyrille Sur, Lili Zhang, Joel B. Schachter, J. Fred Hess, Harold G. Selnick, David J. Vocadlo, Ernest J. McEachern, Jason M. Uslaner, Joseph L. Duffy, Sean M. Smith

MRL, Merck & Co., Inc., Kenilworth, New Jersey, USA (X.W., W.L., J.M., M.P., L.S., K.S., G.T., J.L., K.K.H., S.X.L., L.H., S.-C.C., D.K., J.P.M., D.J.R., X.M., E.H., C.S., L.Z., J.B.S., J.F.H., H.G.S., J.M.U., J.L.D., S.M.S.); Alectos Therapeutics Inc., Burnaby, British Columbia, Canada (D.J.V., E.J.M.)

Supplemental Figures

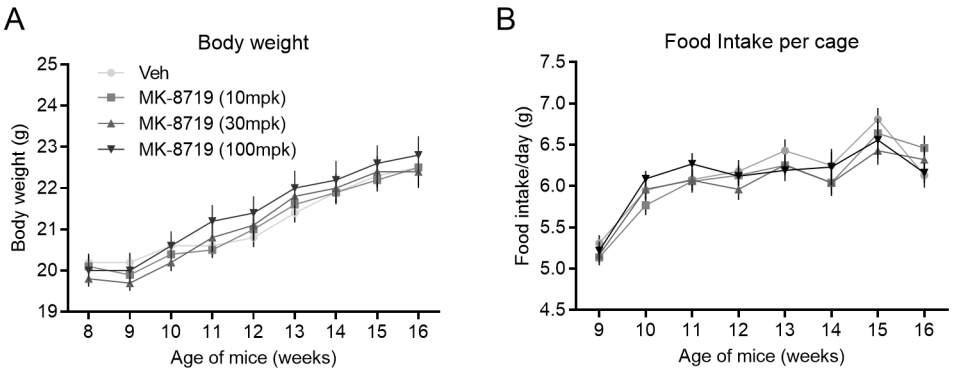

Supplemental Figure 1. Effects of chronic treatment of rTg4510 mice with MK-8179 on body weight and food intake. rTg4510 mice were treated with vehicle or MK-8719 at 10, 30, and 100 mg/kg in diet from 8 to 16 weeks of age. Body weight (A) and food intake (B) were monitored weekly. Animals in all groups increased in body weight and food intake during the treatment period ($p<0.001$), but no significant difference was observed between the treatment groups (body weight, $p = 0.13$, food intake, $p = 0.37$). (n=56/group, two-way ANOVA).

Supplemental Tables

Compound	hOGA Ki (nM)	rOGA cell EC50 (nM)	hHEX A/B Ki (µM)	hNAGLU Ki (µM)
MK-8719	7.9	52.7	> 1000	> 1000

Supplemental Table 1. Potency and selectivity of MK-8719. hOGA Ki = human OGA enzyme Ki value; rOGA cell EC_{50} = rat cellular OGA EC_{50} value; hHEX A/B Ki = human HEX A/B enzyme Ki value; hNAGLU Ki = human NAGLU enzyme Ki value.